Yu *et al.*
Low-carbon Materials and Green Construction (2023) 1:4
https://doi.org/10.1007/s44242-022-00003-1

Low-carbon Materials
and Green Construction

ORIGINAL ARTICLE Open Access

Degradation of limestone calcined clay cement (LC^3) mortars under sulfate attack

Cheng Yu[1*], Zhen Li[1] and Jiaping Liu[2]

Abstract

Limestone Calcined Clay Cement (LC^3 is a newly proposed low-carbon cement, which can effectively reduce energy consumption and carbon emissions of the traditional cement industry without changing the basic mechanical properties of cement-based materials. In this study, the degradation process of mortar samples of limestone and calcined clay cementitious material under sulfate attack is studied by both macroscopic and microscopic analysis. The results show that compared with pure Portland cement, the addition of calcined clay and limestone can significantly reduce the expansion rate, loss of dynamic modulus and mass loss of mortar specimens under sulfate attack. The addition of calcined clay and limestone will refine the pore size distribution of mortar specimens, then inhibiting the diffusion of sulfate and formation of corrosive products, therefore leading to a significant improvement of the sulfate resistance.

Keywords Limestone Calcined Clay Cement (LC^3), Sulfate attack, Expansion, Sulfate penetration profiles, Corrosion product

摘要

石灰石-煅烧粘土水泥是一种新型的低碳水泥体系，其力学性能与传统硅酸盐水泥相比，可以有效降低水泥生产过程的中的能耗与碳排放。本文采用宏观测试与微观表征相结合的方法，研究了石灰石-煅烧粘土水泥砂浆在硫酸盐侵蚀作用下的劣化规律，结果表明相较于纯硅酸盐水泥体系，掺入石灰石与煅烧粘土可以显著减少硫酸盐侵蚀作用下砂浆试件的膨胀率和动弹性模量损失，延缓砂浆试件的劣化过程。这主要是由于煅烧粘土与石灰石的加入会细化砂浆的孔隙结构，有效抑制硫酸盐向试件内部的传输与扩散，从而显著降低钙矾石、石膏等导致膨胀的侵蚀产物的生成，提升砂浆试件的抗硫酸盐侵蚀能力。

关键词 石灰石-煅烧粘土低碳复合水泥，硫酸盐侵蚀，膨胀，硫酸根离子扩散，侵蚀产物

1 Introduction

Portland cement (PC) is the largest manufactured product on earth. The production of Portland cement clinker requires heating the basic raw materials limestone and clay to 1,450 °C. The manufacture of 1 ton of cement clinker releases around 860 kg CO_2. Fossil fuel combustion is responsible for around 40% of total CO_2 emissions, while limestone decomposition during calcination is responsible for the remainder [1, 2]. The CO_2 emissions in the production has been up to about 7% of the human activity in the worldwide [3]. In 2020, 2.377 billion tons of Porltand cement is produced in China, which is responsible for around 1.23 billion tons CO_2 emission. Reducing the amount of CO_2 emission during the Portland cement is an important and enduring challenge. As a mature and effective solution to realize low-carbon development of cement industry, supplementary cementitious materials (SCMs), mainly fly ash and ground blast furnace slag,

*Correspondence:
Cheng Yu
yucheng@cnjsjk.cn
[1] State Key Laboratory of High Performance Civil Engineering Materials, Sobute New Materials Co., Ltd, Nanjing 211103, China
[2] School of Materials Science and Engineering, Southeast University, Nanjing 211189, China

are extensively applied in cement and concrete to replace Portland cement to reduce the energy consumption and carbon emissions in the process of cement production and application. However, due to their natural disadvantages like low production, regional disparity distribution, fluctuations in performance and so on, traditional SCMs can not fully meet the demand of high performance and low carbon emission of cement and concrete materials. Limestone calcined clay cement (LC^3) is one developed ternary blended cement that incorporates limestone and calcined clay replacing up to 50% of the Portland cement clinker, which was proposed by Scrivener from EPFL in 2012 [4]. LC^3 has been regarded as a new and potential low-carbon cement solution, owing to its advantages of wide availability of raw materials, low carbon emissions in production, similar production process to Portland cement and so on [4–7]. Compare to PC, LC^3 cement can reduce CO_2 emissions up to 30–40% per ton of cement production [7].

When clay minerals were calcined in the range of 600-900 °C, due to the dehydroxylation, the lattice structure of kaolin component was decomposed to form calcined clay [8–10]. Metakaolin is the main mineral component of calcined clay which has a high pozzolanic reactivity [11, 12]. Metakaolin can react with $Ca(OH)_2$ to form calcium silicoaluminate hydrate gel (C-A-S–H) in cement paste, which could optimize the pore structure, and then improve he mechanical properties and durability [13, 14]. Limestone is beneficial to the early strength development of cement when it is added at a low proportion [15, 16]. A suitable amount of limestone plays a role of "filling effect" and "nucleating effect" in accelerating the early stage of hydration [17–19]. Besides, limited amount of limestone can react with C_3A to form carbon aluminate hydrate [20, 21]. When calcined clay and limestone were added simultaneously, activated aluminum oxide in clay would react with limestone, calcium hydroxide to form single carbon aluminates and half carbon calcium aluminates [22, 23]. It would refine the pore size and the dosage of cement clinker would be decreased without influencing mechanical properties of cement-based material.

Most results show that the 28-day compressive strength of LC^3 is similar to that of an OPC produced using a similar clinker, there is some variation in the results at other ages. While the 3-day strength of LC^3 is slightly lower than that of OPC and similar to that of slag or fly ash blended cements. By 7 days, the strength of LC^3 has been reported to be similar to or higher than that of OPC [6]. The strength of LC^3 is strongly related to the kaolinite content in clay [24]. Also, parameters such as the particle sizes of the individual components, the composition of the clinker, temperature and alkali content play an important role on strength development of LC^3[24–27].

Some research has shown that calcined clay and limestone composite cementitious material system can reduce the diffusion coefficient of chloride ion of concrete [28]. Also, the study by Shi showed that calcined clay – limestone Portland cement blends exhibit a comparable sulfate resistance to those of sulfateresisting cements [29]. However, the main hydration product of LC^3—calcium carbonaluminate also has the potential to react with sulfate to form ettringite. Moreover, a large amount of aluminum phase in calcined clay has been introduced, which could also react with sulfate ions afterwards. Therefore, the sulfate resistance of Limestone Calcined Clay Cement for a long term and the reaction between sulfate and hydration product containing aluminate needs to be further investigated. In this study, expansion rate and dynamic modulus of mortar exposed to sodium sulfate solution were investigated. Mortars made by pure Portland cement, Portland cement blended with fly ash and slag, and limestone calcined clay cement are involved in this study. Corrosion products were analyzed by XRD semi-quantitative method and elementary mapping to identify the potential reaction between penetrated sulfates and hydration product.

2 Materials and experimental methods

2.1 Materials

In this study, P·I 42.5 Portland cement (PC) and China ISO Standard Sand are used. Calcined clay (CC) is provided by India Low Carbon Cement Project team. Limestone (LS), Fly ash (FA), slag (SL) are provided by Sobute New Materials Co., Ltd. The chemical composition of cement, calcined clay, limestone, fly ash and slag is shown in Table 1.

The particle size distribution of raw materials was shown in Fig. 1. The fineness of the calcined clay particles is larger than cement and similar to fly ash and limestone powders. Also, calcined clay exhibits a higher proportion

Table 1 Chemical composition of raw materials by XRF

Mass fraction /%	SiO_2	Al_2O_3	Fe_2O_3	CaO	MgO	SO_3	Na_2O	K_2O	TiO_2
Portland cement (PC)	18.50	4.42	3.25	62.13	2.45	2.88	0.12	0.59	0.34
Calcined clay (CC)	51.7	42.1	3.02	0.205	-	0.056	0.113	0.231	2.22
Limestone (LS)	1.22	1.18	0.367	96.4	0.121	0.048	-	0.107	-
Fly ash (FA)	50.2	28.6	6.21	7.31	1..30	0.969	0.822	1.42	1.36
Slag (SL)	30.9	15.9	.0281	41.5	6.86	2.58	0.316	0.335	0.633

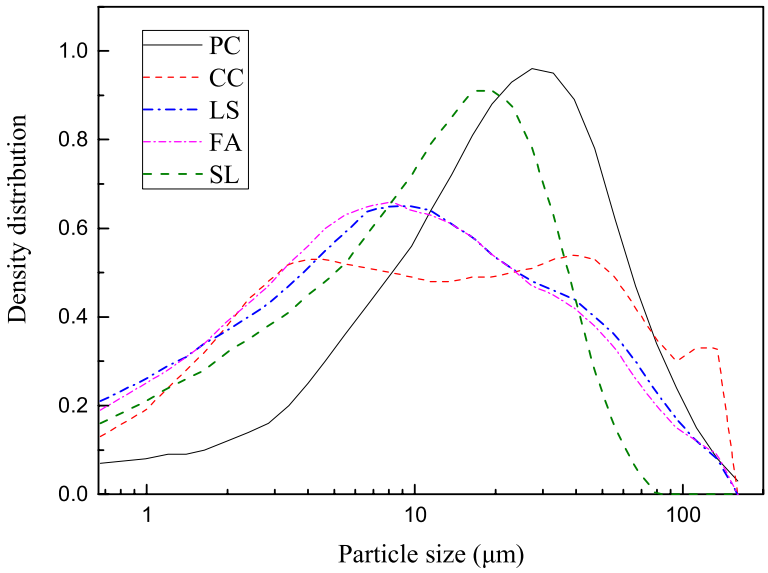

Fig. 1 Particle size distribution of raw materials

for particles size larger than 100 μm. This is due to agglomeration of clay particles, of which the morphologies are different from clinker and SCMs particles.

The crystalline phase composition phase of calcine clay and cement investigated by XRD are shown in Fig. 2. The crystalline phases of calcined clay are quartz and undehydrated kaolinite. The most reactive component in calcined clay is metakaolin, which is an amorphous phase.

2.2 Mix proportion

In calcined clay and limestone composite cementitious material system, the mass ratio of calcined clay and limestone is fixed as 2:1. The replacement ratio of calcined

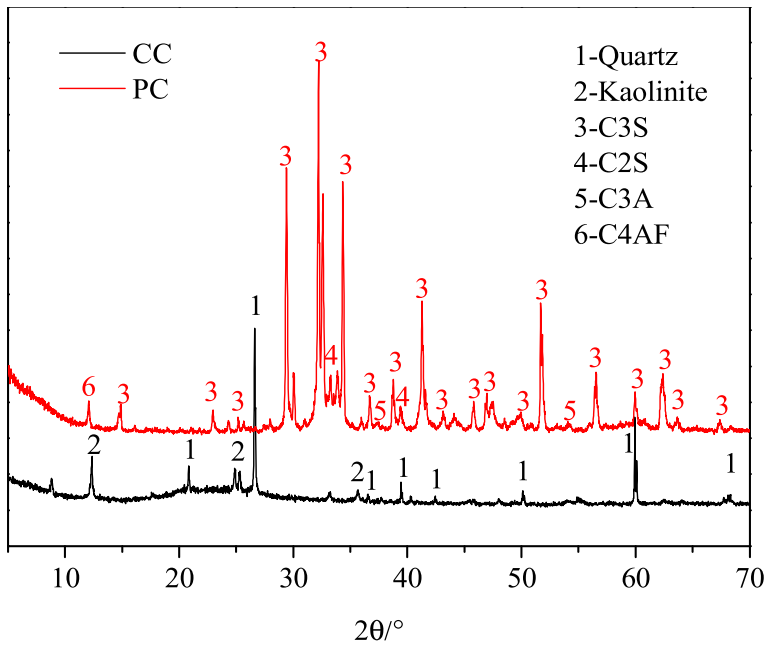

Fig. 2 XRD patterns of raw materials

clay and limestone of Portland cement is 15% (LC15), 30% (LC30) and 45% (LC45). Pure Portland cement (PC) and a traditional SCMs replacement system (SF, 10% fly ash and 20% slag) are also applied as reference group. The water to binder ratio of mortar specimens 0.6. The ratio of cementitious material to sand is fixed to 1:3. The mix proportions are given in Table 2. Mortar sample with a size of 40 mm × 40 mm × 160 mm were cast and demoulded after 24 h, and then cured in lime water for 28 days with a temperature of 20 ℃.

2.3 Sulfate immersion test

Copper crews were pre-embedded at both ends of mortar specimens used for sulfate immersion test. The original laitance on the surface of specimens were removed to accelerate ion penetration rate and control the experimental error. Afterwards, specimens were immersed in 5wt-% sodium sulfate solution. The volume ratio of solution to specimens was 10 and the temperature was around 20 °C. Sulfate solution was renewed every 30 days.

The dynamic modulus of mortar specimens at different immersion ages was tested by nonmetal ultrasonic detector according to GB/T 50082–2009 on the vertical direction of samples.

The expansion of specimens was measured by JD18 length measuring instrument and values were accurate to 0.001 mm. The expansion rate of mortars was calculated by the following formula (1) with average value of three specimens.

$$E_T = L_T - L_0/140 \times 100\% \quad (1)$$

In the formula, E_T-The expansion rate of specimens at an immersion age of T (%), L_T-The length of specimens at an immersion age of T (mm), L_0- The initial length of specimens (mm).

2.4 X-ray Diffraction (XRD)

2.4.1 Phase analysis of pastes before sulfate attack

The cement paste was prepared through a same procedure as above mentioned and then cured in standard curing chamber. After a certain time of curing, a slight piece of cement paste was cut and immersed in isopropanol from 48 h to stop hydration. Then the sample was dried in a vacuum oven for another 48 h at 40 °C, and grounded to powders afterwards. The dry powders of cement paste were than measured by X-ray diffraction (XRD). 10wt-% corundum was pre-mixed as internal standard to realize the quantification by Rietveld analysis. The diffraction data was collected by using Bruker D8 Discover X diffractometer in a θ-θ configuration employing CuKα radiation (λ = 1.54 Å) with a fixed divergence slit size 0.5°. The powder samples were scanned between 5 and 70° using a step size of 0.02° with scanning speed of 0.3 s/step. The software used for Rietveld refinement was TOPAS from Bruker AXS.

2.4.2 Phase analysis of mortars after immersed in sulfate solution

After immersed in solution for 90 d and 180 d, a slice with 2 mm wide was cut from the surface of mortar specimens. Then the slice was grounded into powders and passed through 200 mesh sieves. Phase analysis was performed by Bruker D8 Advance X-ray Diffractometer. The samples were scanned on a rotating stage between 5 and 20° using a step size of 0.02° with time per step of 0.5 s.

2.5 SEM elemental mapping for sulfate penetration profiles

The slices of mortar samples were also examined by scanning electron microscopy SEM (FEI Quanta 200) using backscattered electron image and EDS X-ray analysis. Sample preparation included drying, impregnation with epoxy resin, cutting, polishing and coating with carbon. The qualitative elemental mappings were obtained at low magnification level (100), with a resolution of 512*400 pixels. However, the elemental qualitative mappings are scaled according to the pixel of major intensity and cannot be simply compared to each other. A code for image analysis has been developed to extract SO_3 profiles from the mappings, which consists of two stages: rescaling and calibration [30].

3 Results

3.1 Mechanical properties

The compressive strength of mortar was tested after curing for 3, 7, 28 and 90 days in standard condition

Table 2 Mix proportions of mortars (g)

Specimen	W/B	PC	FA	SL	CC	LS	Water	Sand
LC15	0.6	382.5	-	-	45	22.5	270	1350
LC30		315	-	-	90	45	270	1350
LC45		247.5	-	-	135	67.5	270	1350
SF		315	45	90	-	-	270	1350
P		450	-	-	-	-	270	1350

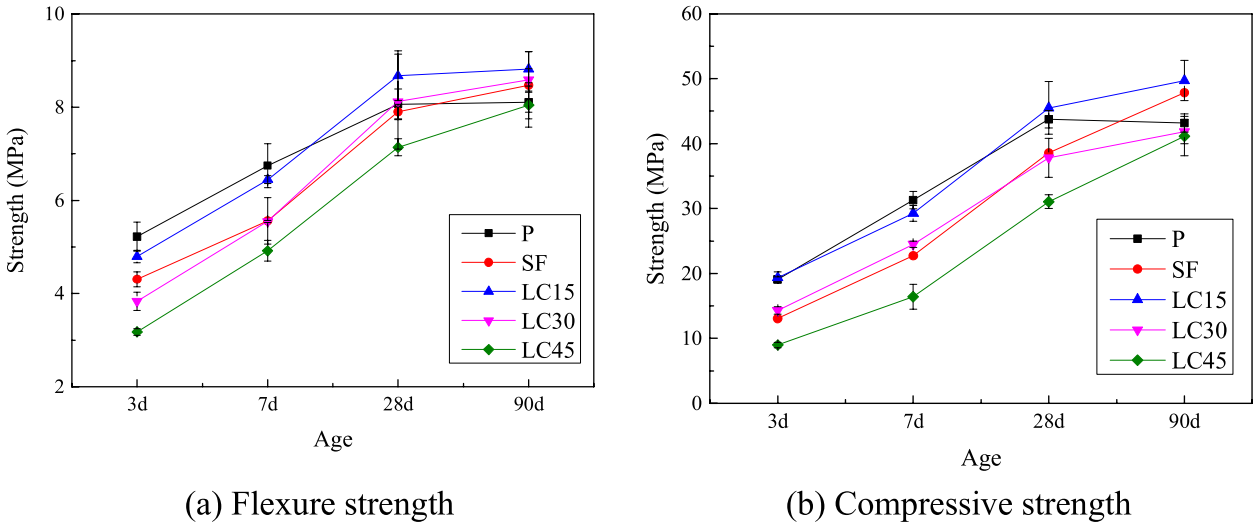

Fig. 3 Strength of mortars at different ages. **a** Flexure strength. **b** Compressive strength

according to Chinese standard GB/T 17671–2021. The flexure and compressive strength of mortars are shown in Fig. 3.

As can be seen in Fig. 3, both of the flexure strength and compressive strength of mortars containing limestone and calcined clay are lower than that of OPC at 3 days and 7 days. The strength at early age also decreased with the increasing content of limestone and calcine clay. The compressive strength of LC45 is only 8.8 MPa at 3 days and 15.4 MPa at 7 days, While the value of P mortars are 19.4 and 31 MPa respectively. At 28 days, the strength of LC15 and LC30 is similar or even a little higher that P mortars. The strength of LC45 is also equal to P at 90 days. Besides, for a same clinker replacement level of 30%, the strength development of LC30 is nearly the same to SF. All these results indicated that despite the addition of limestone and calcined clay will reduce the early age strength of mortars, it will not bring any negative effect on the long-term strength.

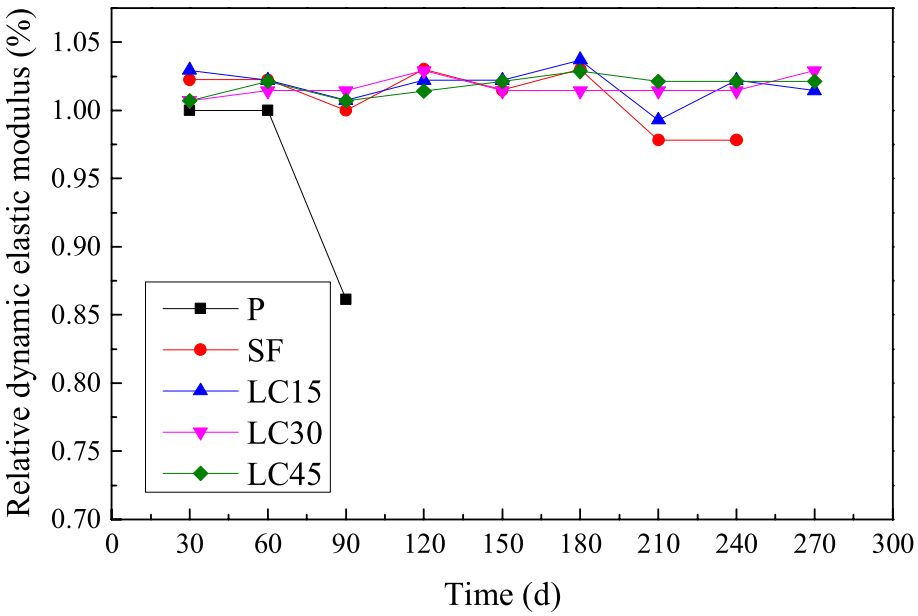

Fig. 4 The relative dynamic modulus of mortars exposed to sulfate solution

3.2 Relative dynamic elastic modulus

The relative dynamic modulus change of mortar specimens is shown in Fig. 4. The relative dynamic modulus of Portland cement mortar has a significant decrease after 90 days, which indicates that the internal microstructure specimens have been damaged under sulfate attack. While the relative dynamic modulus of mortar specimens with limestone and calcine clay remains unaltered. It can be inferred that the addition of calcined clay and limestone refine the pore size distribution of mortars, which could prevent the penetration of sulfate ions into mortars. Therefore, the deterioration that caused by sulfate attack occurs only at the surface of LC Mortars. And the internal structure remains unaltered after 270 days exposure.

3.3 Expansion

Figure 5 shows the expansion rate of mortar specimens under sulfate attack. The expansion rate of P mortar specimen shows a steady increase after 30 days exposure, and reaches 2.5% at 210 d. The SF mortar also starts to expand after 240 d. While the addition of calcined clay and limestone significantly reduce the expansion rate of mortars. The expansion rate of LC15, LC30 and LC45 are 0.016%, 0.007% and 0.001% respectively after 270 d exposure. The expansion of SF mortar is similar to LC mortars so far.

4 Phase analysis by XRD

4.1 Hydration products

The XRD patterns of pastes sample after 3 days hydration is shown in Fig. 6, and the phase composition acquired by XRD Rietveld quantitative analysis are listed in Table 3. As can be seen in Table 3, there are still a certain amount of unhydrated clinker in the samples. The P sample shows a highest portlandite amount among the five samples. Adding limestone and calcined clay will reduce the content of portlandite due to the pozzolanic reaction.

The XRD patterns of pastes sample after 28 days hydration is shown in Fig. 7, and the phase composition are listed in Table 4. First of all, the amount of unhydrated clinker in the samples are quite low after 28 days. Apart from the portlandite and ettringite, both hemicarboaluminate(Hc) and Monocarboaluminate(Mc) are detected in the LC samples. Moreover, the content of both Hc and Mc increases with the amount of limestone and calcined clay. Meanwhile, the amount of calcite is reduced compare to 3 days. That means the aluminate in the calcined clay will react with limestone to form calcium carboaluminate phases. More importantly, the amount of ettringite dose not change significantly from 3 to 28 days, which indicates that the aluminate prefers to go to Hc and Mc, rather than Ettringite.

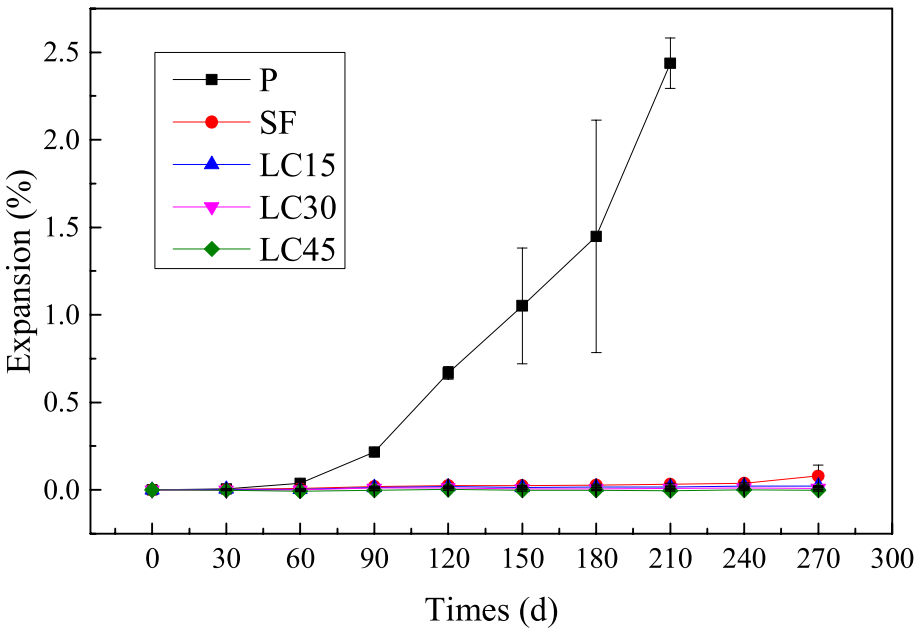

Fig. 5 Expansion of mortars exposed to sulfate solution

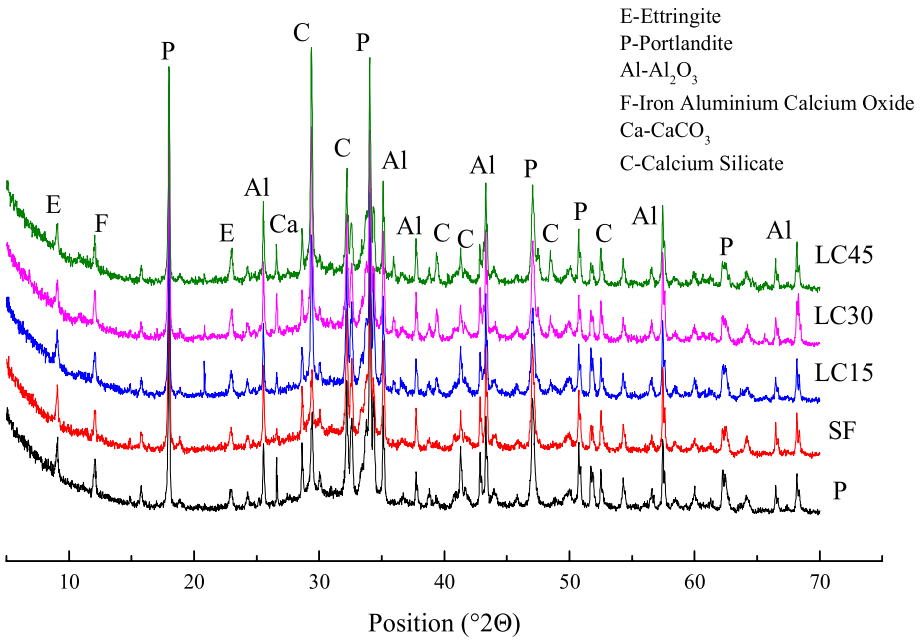

Fig. 6 XRD patterns of pastes at 3d

Table 3 Phase composition of pastes acquired by XRD quantitative analysis at 3 days (wt-% of the paste)

Specimen	C_3S	C_2S	C_4AF	Portlandite	Ettringite	Calcite
P	11.7	3.3	8.9	9.5	2.8	1.5
SF	6.8	3.2	7.8	7.8	2.5	1.3
LC15	11.7	2.2	8.3	7.2	2.3	4.7
LC30	7.1	2.4	6.6	6.6	1.7	6.2
LC45	6.5	2.1	7.1	7.2	2.2	7.9

4.2 Corrosion products

The relative amount of main hydration product and corrosion products of mortars can be analyzed by XRD. The characteristic peak of quartz is 26.59° for X-ray Diffraction, to avoid the interference of the quartz, the range of diffraction patterns is selected from 5° to 20°. The characteristic diffraction peak (2θ) that corresponds to monocarboaluminate (Mc), hemicarboaluminate (Hc), portlandite (CH), ettringite (Ettr.) and gypsum (Gyp.) are 11.67°, 10.78°, 18.01°, 9.09° and 11.59° respectively. Figure 8 is the XRD pattern of center part of mortars, which are not affected by the sulfate ions yet, after 90 days exposure. From the patterns, it is clear that the hydration products of LC mortars are different compared with P and SF mortars. Besides ettringite and portlandite, monocarboaluminate, hemicarboaluminate appears after 90 days. Moreover, the amount Mc and Hc are increased with increasing amount of calcined clay and limestone. Figure 9 shows the XRD pattern of surface part of mortars after 90 days exposure. Compared with patterns of center part, it is obvious that more ettringite and gypsum have been formed in the surface part of mortar specimens after 90 days exposure in sulfate solution. The monosulfate and portlandite are reacting with incoming sulfate to form ettringite and gypsum, the amount of ettringite and gypsum formed in LC mortars are lower than P and SF samples. This indicates that the addition of calcined clay and limestone could mitigate the forming of corrosion product by sulfate ingress. It is well known that the expansion of mortars under sulfate attack is mainly due to the crystallization of ettringite. LC mortars shows less ettringite forming, thereby leading to a reduce expansion rate and macro degradation. This explains why LC mortars shows lower expansion rate and dynamic modulus loss than P and SF samples.

Figures 10 and 11 show the XRD pattern of center and surface part of mortars after 180d exposure respectively.

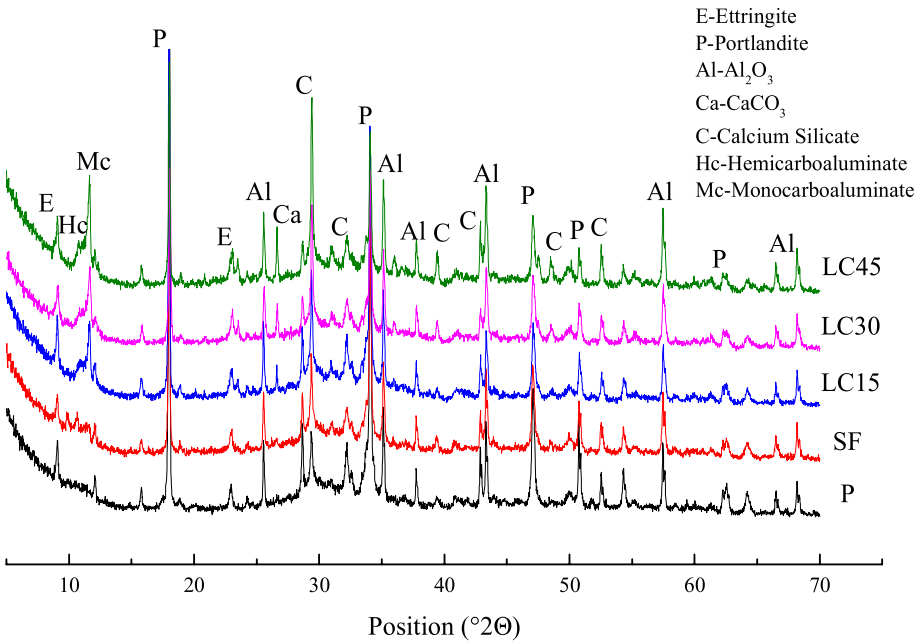

Fig. 7 XRD patterns of pastes at 28

Table 4 Phase composition of pastes acquired by XRD quantitative analysis at 28 days (wt-%)

Specimen	C_3S	C_2S	C_4AF	Portlandite	Mc	Hc	Ettringite	Calcite
P	4.4	1.2	3.7	14.5	0	0	3.9	1.4
SF	1.4	1.1	3.4	9.0	0	1.3	3.2	2.9
LC15	2.0	2.7	3.9	9.8	5.6	1.4	3.2	2.0
LC30	2.0	2.3	3.7	6.9	7.0	1.3	2.5	3.5
LC45	1.6	2.6	3.3	4.8	8.0	1.4	2.1	4.6

It can be seen that the amount of ettringite and gypsum increases with the exposure time. After 180 days, nearly all the monosulfate and portlandite have been consumed to form the corrosion product. Ettringite is also forming in the center of P mortars, which indicates that the center has already been affected by the incoming sulfate through cracks. Moreover, in the surface of LC mortars, the amount of Hc and Mc are reduced compare to center samples. This infers that the Hc and Mc can also react with sulfate ions to form ettringite.

As can been seen from all the patterns, the formation of ettringite and gypsum are significantly reduced by adding calcined clay and limestone. Due to the high pozzolanic reactivity, calcined clay can react with limestone to form mono- and hemi-carboaluminate, leading to a refined pore structure [31]. The optimization of microstructure could strongly mitigate the penetration of corrosive ions, like chloride ion and sulfate ions, which leads to an improved sulfate resistance.

4.3 Sulfate penetration profiles by elemental mapping

Figures 12, 13, 14, 15, 16 show the BSE image, S-Mapping, and sulfate profiles of mortar samples immersed in sulfate solution for 180 days. As seen from the BSE image, Both P, SF and LC15 samples show clear mass loss at the surface, where the aggregates become exposed due to the disintegration of surrounding cement paste. While the surface of LC30 and LC45 samples remains in a relatively good shape. Moreover, the original surface of P and SF mortar is nearly removed and cracks are propagating in the region close to fresh surface. This brings some uncertainty in the following sulfate penetration profiles acquisition concerning the depth from the original surface.

From the sulfur mapping, it can be clearly seen that sulfate-bearing phases forming around aggregates in the surface region is observed in all three samples. According the chemical nature of sulfate attack, these sulfate bearing phases are mainly gypsum and ettringite [32]. The brightness of red color is in direct proportional to the

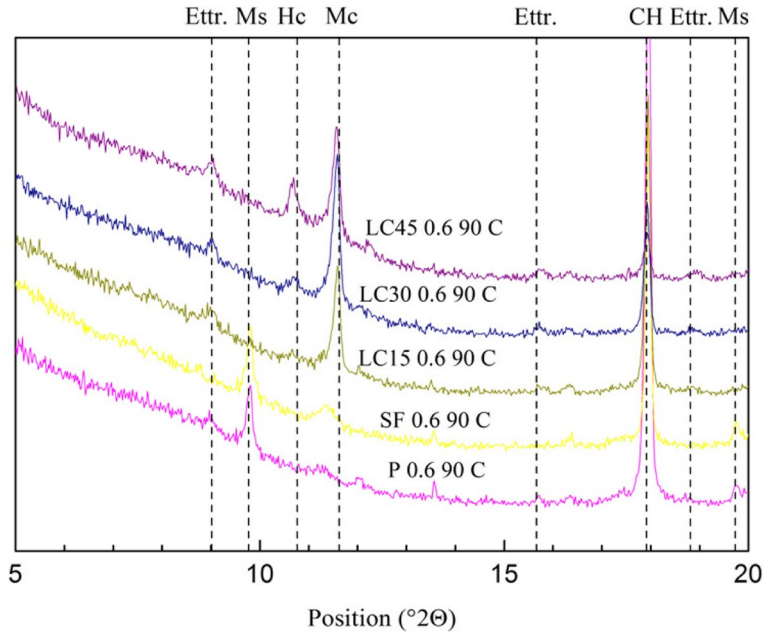

Fig. 8 XRD patterns for the center of the mortars at 90 days

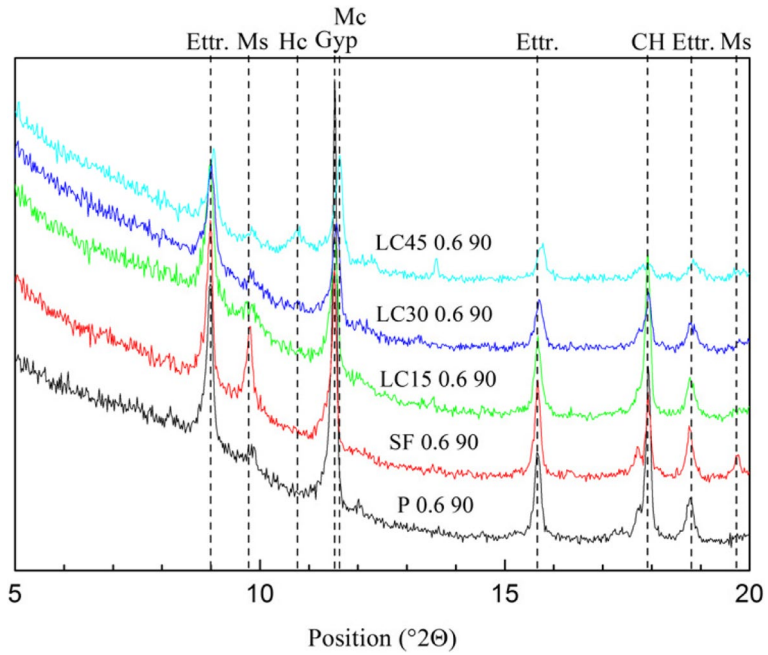

Fig. 9 XRD patterns for the surface of the mortars at 90 days

sulfate concentration in this area. It is obvious that the amount of sulfate bearing product that formed through sulfate ingress in P and SF samples are much higher that LC samples. Also, the amount of sulfate corrosion product is reduced with the increasing replacing ratio of calcined clay and limestone.

As seen from the sulfate profiles, P mortars show higher sulfate content at the penetration depth of 1 ~ 2 mm. The SO_3 content reaches around 10%, which indicated that significant gypsum deposits found in cracks near the surface. SF mortar exhibited a deeper sulfate penetration depth and even higher sulfate content than P mortar.

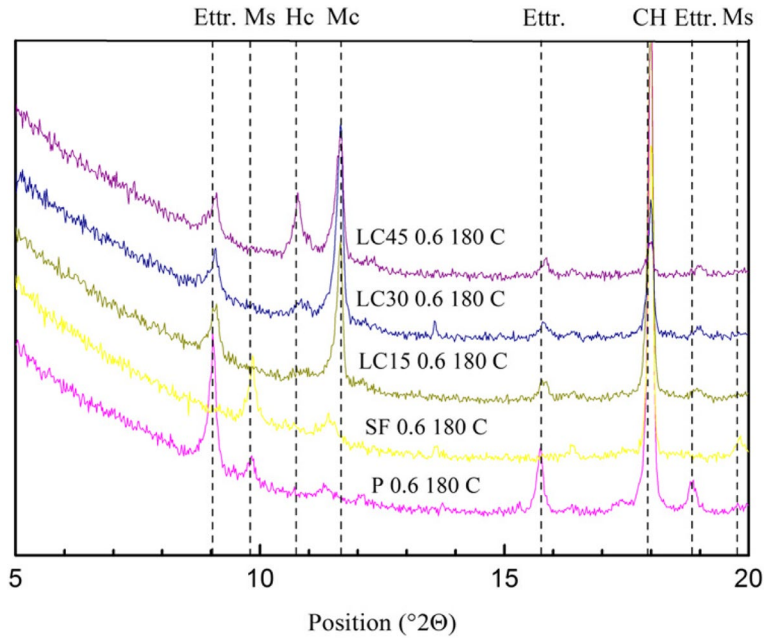

Fig. 10 XRD patterns for the center of mortars after 180 days

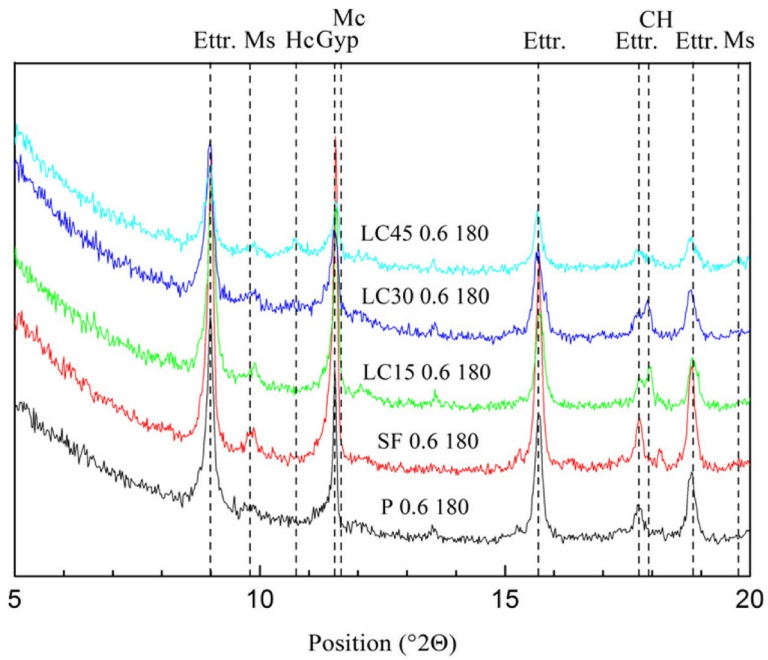

Fig. 11 XRD patterns for the surface of mortars after 180 days

The sulfate content exceeds 8% from the depth 1.5 mm to 3.5 mm. This is probably because the sulfate immersion test of mortars started just after 28 days curing, when the pozzolanic reaction of slag and fly ash is not sufficient for providing a dense microstructure to against sulfate penetration. The sulfate profiles of LC mortars exposed to sodium sulfate solutions have no significant difference in the penetration depth, in which the sulfate contents are assembled in the region before 2 mm depth from surface. However, LC15 sample shows a higher peak at around 1 mm depth than LC30 and LC45, indicating more sulfate bearing phases forming.

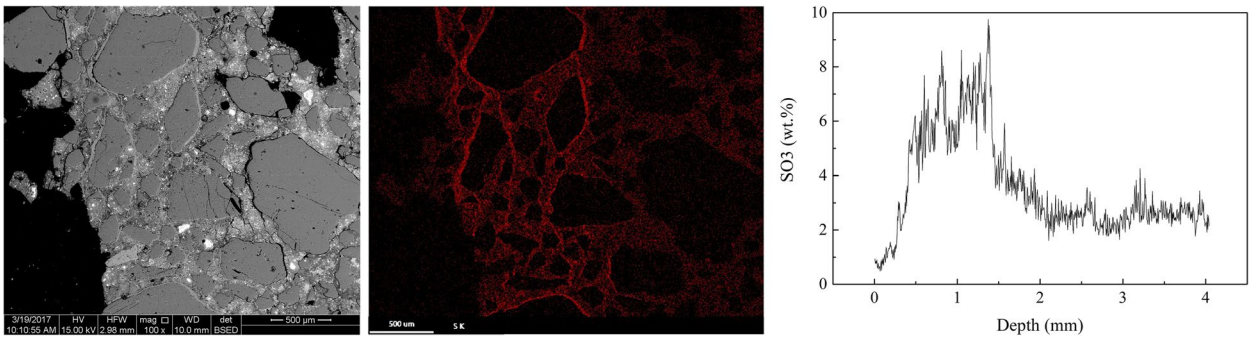

Fig. 12 Sulfate profiles of P specimen acquired by SEM-mapping

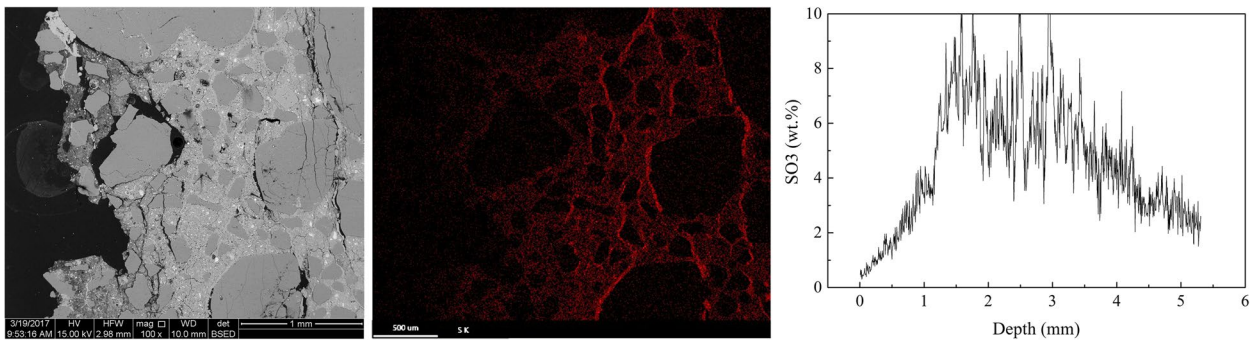

Fig. 13 Sulfate profiles of SF specimen acquired by SEM-mapping

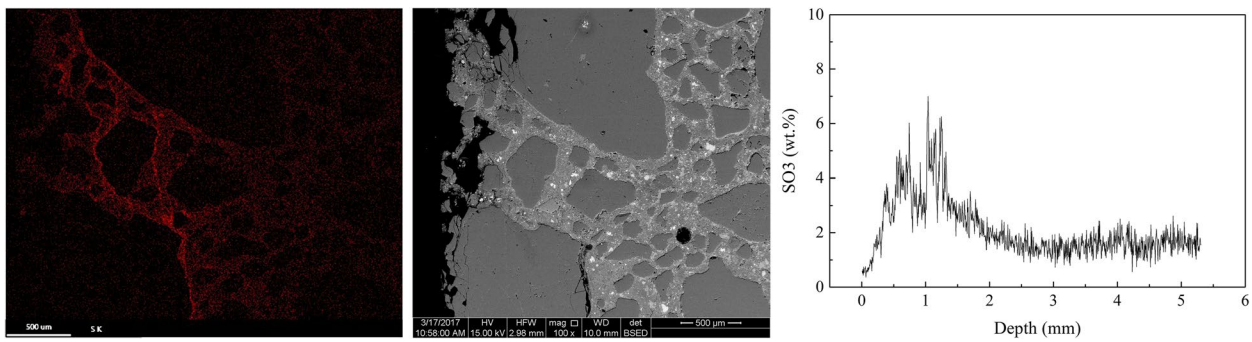

Fig. 14 Sulfate profiles of LC15 specimen acquired by SEM-mapping

The comparison of sulfate profiles in P, LC15, LC30 and LC45 specimens are shown in Fig. 17. It is quite clear that both the sulfate penetration depth and amount of sulfate bearing phases are reduced with the addition of calcined clay and limestone. The resistance against sulfates increases as replacement of clinker with limestone and calcined clay is increased.

As can be seen from the Fig. 18, the addition of calcined clay and limestone will refine the pore structure and also reduce the porosity when the replacement level is 15% and 30%. When the replacement level reaches to 45%, the porosity is high than Portland cement, however, the pore size distribution is also refined, owing the addition of calcined clay and limestone. This is coincidence with results of strength, and also the studies by other researchers [31, 33, 34]. Therefore, despite there are remains the potential harmless nature of the conversion of mono or hemi-carboaluminate to ettringite during sulfate attack, the LC mortars shows an improve resistance to sulfate attack that Portland cement and other SCMs

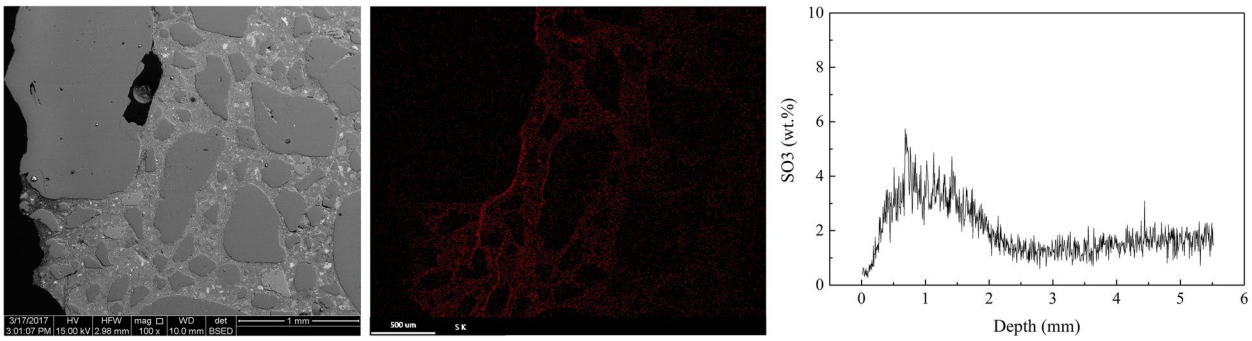

Fig. 15 Sulfate profiles of LC30 specimen acquired by SEM-mapping

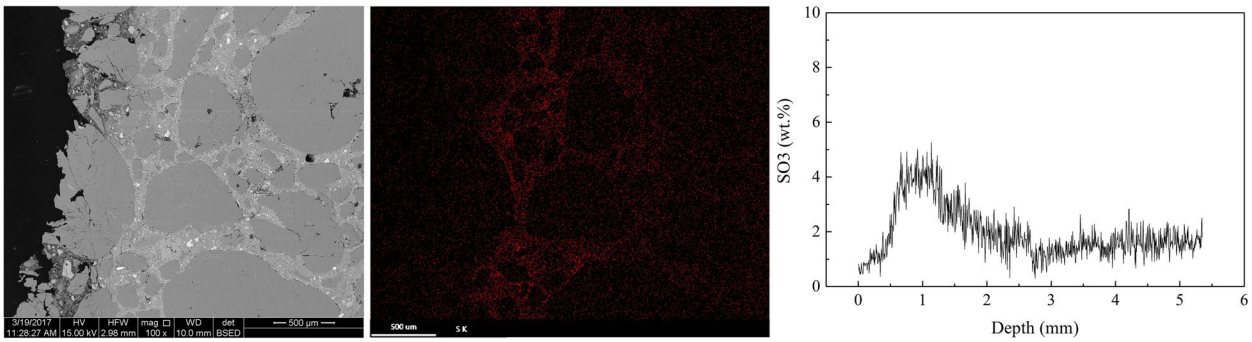

Fig. 16 Sulfate profiles of LC45 specimen acquired by SEM-mapping

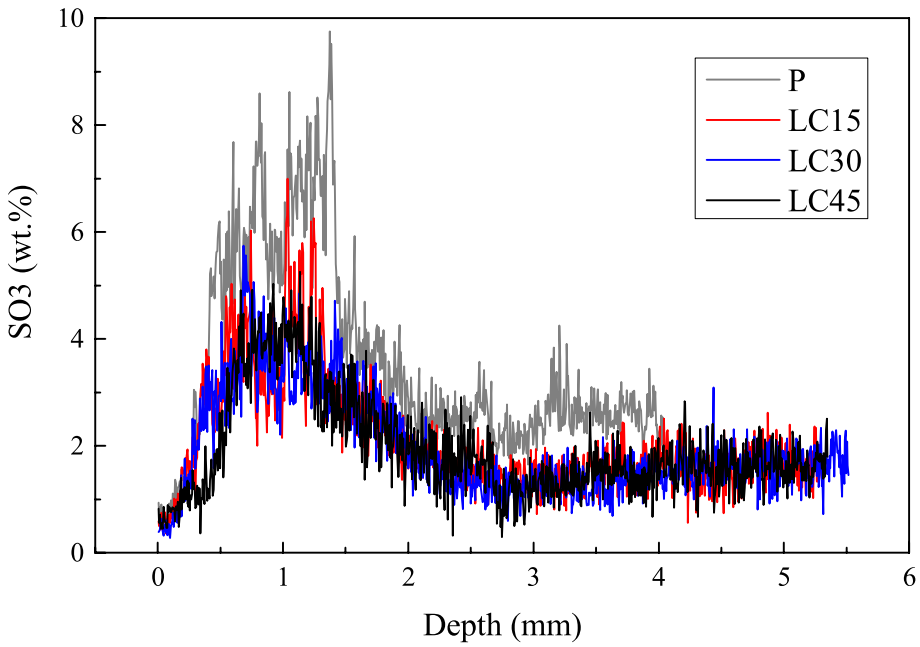

Fig. 17 Sulfate profiles of P, LC15, LC30 and LC45 specimens

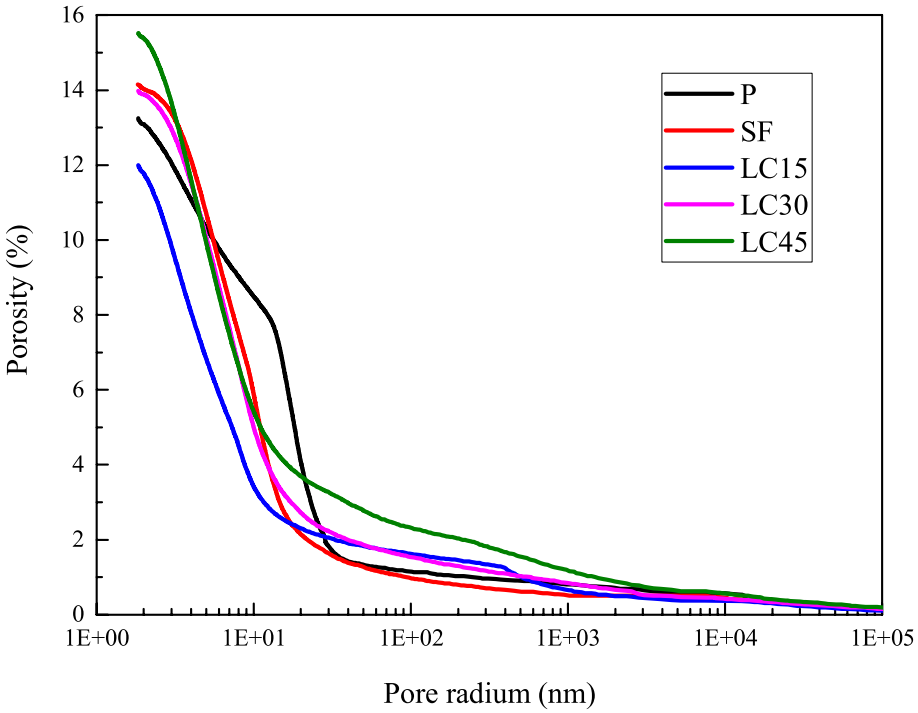

Fig. 18 Pore size distribution of P, LC15, LC30 and LC45 specimens after 28 days curing

due to a lower permeability that induced by refined pore-structure. Also, the finer pore-structure in LC^3 develops earlier than slag and fly ash system.

5 Conclusions

(1) Despite the addition of limestone and calcined clay will reduce the early age strength of mortars, it will not bring any negative effect on the long-term strength.
(2) Partial replacement of calcined clay and limestone to Portland cement can reduce expansion rate and dynamic modulus loss of mortars under sulfate attack for 270 days.
(3) Both the sulfate penetration depth and amount of sulfate bearing phases are reduced with the addition of calcined clay and limestone. And the resistance against sulfates increases as replacement of clinker with limestone and calcined clay is increased.
(4) Reactive alumina in calcined clay can react with limestone, calcium hydroxide to form mono- and hemi-carboaluminate to get a refined pore structure. Although mono or hemi-carboaluminate can react with sulfate to form ettringite, the improvement of impermeability ensures LC mortars an improved sulfate resistance.

Acknowledgements
We appreciated Peng Yuan participated part of the experiments in this manuscript

Authors' contributions
Cheng Yu performed the experiments and is responsible for the major part of writing. Zhen Li responsible for performing experiments and collecting the literatures for the manuscript. Jiaping Liu is responsible for the writing and revising of this manuscript. All authors read and approved the final manuscript.

Funding
This study was supported in part by grants from National Natural Science Foundation of China (52278259).

Availability of data and materials
All data generated or analyzed during this study are included in this published article.

Declarations

Competing interests
The authors declare that they have no competing interests.

Received: 30 September 2022 Revised: 18 November 2022 Accepted: 20 November 2022
Published online: 01 February 2023

References

1. Monteiro, P. J. M., Miller, S. A., & Horvath, A. (2017). Towards sustainable concrete. *Nature materials, 16*(7), 698–699.
2. Environment, U. N., Scrivener, K. L., John, V. M., et al. (2018). Eco-efficient cements: Potential economically viable solutions for a low-CO2 cement-based materials industry. *Cement and Concrete Research, 114*, 2–26.

3. Ritchie H., Roser M. CO_2 and greenhouse gas emissions. (2020). https://ourworldindata.org/co2-and-other-greenhouse-gas-emissions [Online Resource]
4. Scrivener, K., Martirena, F., Bishnoi, S., et al. (2018). Calcined clay limestone cements (LC^3). *Cement and Concrete Research, 114*, 49–56.
5. Jiang G., Rong Z., Sun W. (2015). Effects of metakaolin on mechanical properties, pore structure and hydration heat of mortars at 0.17 w/b ratio. *Construction and Building Materials*, *93*, 564–572.
6. Li, Q., Geng, H., Shui, Z., et al. (2015). Effect of metakaolin addition and seawater mixing on the properties and hydration of concrete. *Applied Clay Science, 115*, 51–60.
7. Sharma, M., Bishnoi, S., Martirena, F., & Scrivener, K. (2021). Limestone calcined clay cement and concrete: a state-of-the-art review. *Cement and Concrete Research, 149*, 106564.
8. Hanein, T., Thienel, K. C., Zunino, F., et al. (2022). Clay calcination technology: State-of-the-art review by the RILEM TC 282-CCL. *Materials and Structure, 55*, 3.
9. Sayanam, R. A., Kalsotra, A. K., Mehta, S. K., et al. (1989). Studies on thermal transformations and pozzolanic activities of clay from Jammu region (India). *Journal of Thermal Analysis and Calorimetry, 35*(1), 99–106.
10. Ambroise, J., Murat, M., & Pera, J. (1986). Investigations on synthetic binders obtained by middle-temperature thermal dissociation of clay minerals. *Silicates industriels, 51*(7–8), 99–107.
11. Sabir, B. B., Wild, S., and Bai, J. (2001). Metakaolin and calcined clays as pozzolans for concrete: a review. *Cement and Concrete Composites, 23*(6), 441–454.
12. Fernandez, R., Martirena, F., & Scrivener, K. L. (2011). The origin of the pozzolanic activity of calcined clay minerals: a comparison between kaolinite, illite and montmorillonite. *Cement and Concrete Research, 41*(1), 113–122.
13. Siddique, R., & Klaus, J. (2009). Influence of metakaolin on the properties of mortar and concrete: A review. *Applied Clay Science, 43*(3), 392–400.
14. FríAs, M., & Cabrera, J. (2000). Pore size distribution and degree of hydration of metakaolin–cement pastes. *Cement and Concrete Research*, *30*(4), 561–569.
15. Tsivilis, S., Chaniotakis, E., Badogiannis, E., et al. (1999). A study on the parameters affecting the properties of Portland limestone cements. *Cement and Concrete Composites, 21*(2), 107–116.
16. Voglis, N., Kakali, G., Chaniotakis, E., et al. (2005). Portland-limestone cements. their properties and hydration compared to those of other composite cements. *Cement and Concrete Composites*, *27*(2), 191–196.
17. Oey, T., Kumar, A., Bullard, J. W., et al. (2013). The filler effect: the influence of filler content and surface area on cementitious reaction rates. *Journal of the American Ceramic Society, 96*(6), 1978–1990.
18. Lothenbach, B., Saout, G. L., Gallucci, E., et al. (2008). Influence of limestone on the hydration of Portland cements. *Cement and Concrete Research, 38*(6), 848–860.
19. Matschei, T., Lothenbach, B., & Glasser, F. P. (2007). The role of calcium carbonate in cement hydration. *Cement and Concrete Research, 37*(4), 551–558.
20. Kakali, G., Tsivilis, S., Aggeli, E., et al. (2000). Hydration products of C_3A, C_3S and Portland cement in the presence of $CaCO_3$. *Cement and concrete Research, 30*(7), 1073–1077.
21. Antoni, M., Rossen, J., Martirena, F., et al. (2012). Cement substitution by a combination of metakaolin and limestone. *Cement and concrete research, 42*(12), 1579–1589.
22. Ingram, K., Poslusny, M., Daugherty, K., et al. (1990). Carboaluminate reactions as influenced by limestone additions. *Proc Carbonate Additions to Cement, 1064*, 14–23.
23. Avet, F., & Scrivener, K. (2018). Investigation of the calcined kaolinite content on the hydration of Limestone Calcined Clay Cement (LC^3). *Cement and Concrete Research, 107*, 124–135.
24. Fernandez, R., Martirena, F., & Scrivener, K. L. (2011). The origin of the pozzolanic activity of calcined clay minerals: a comparison between kaolinite, illite and montmorillonite. *Cement and concrete research, 41*(1), 113–122.
25. Krishnan, S., Singh, A., & Bishnoi, S. (2021). Impact of Alkali Salts on the Hydration of Ordinary Portland Cement and Limestone-Calcined Clay Cement. *Journal of Materials in Civil Engineering, 33*(9), 04021223.
26. Mishra, G., Emmanuel, A. C., & Bishnoi, S. (2019). Influence of temperature on hydration and microstructure properties of limestone-calcined clay blended cement. *Materials and Structures, 52*(5), 1–13.
27. Yu, J., Wu, H. L., Mishra, D. K., et al. (2021). Compressive strength and environmental impact of sustainable blended cement with high-dosage Limestone and Calcined Clay (LC2). *Journal of Cleaner Production, 278*, 123616.
28. Maraghechi, H., Avet, F., Wong, H., et al. (2018). Performance of Limestone Calcined Clay Cement (LC^3) with various kaolinite contents with respect to chloride transport. *Materials and structures, 51*(5), 1–17.
29. Shi, Z., Ferreiro, S., Lothenbach, B., et al. (2019). Sulfate resistance of calcined clay–Limestone–Portland cements. *Cement and Concrete Research, 116*, 238–251.
30. Yu C, Sun W, Scrivener, K. (2014). Application of Image Analysis Based on SEM and Chemical Mapping on PC Mortars under Sulfate Attack. Journal of Wuhan University of Technology(Materials Science Edition), *3*, 6.
31. Parashar, A., & Bishnoi, S. (2021). Hydration behaviour of limestone-calcined clay and limestone-slag blends in ternary cement. *RILEM Technical Letters, 6*, 17–24.
32. Zunino F. (2020). Limestone Calcined Clay Cements (LC^3): Raw Material Processing, Sulfate Balance and Hydration Kinetics. École Polytechnique Fédérale de Lausanne (EPFL), Switzerland.
33. Antoni M. (2012). Investigation of cement substitution by blends of calcined clays and limestone. École Polytechnique Fédérale de Lausanne (EPFL), Switzerland.
34. Zunino F, Martirena F, Scrivener K. (2021). Limestone Calcined Clay Cements (LC^3). *ACI Materials Journal*, *118*(3), 49–90.

Publisher's Note